

Phase field modelling of the growth and detachment of bubbles in a hydrogen electrolyzer

Carlos Uriarte

Área de Electromagnetismo, Universidad Rey Juan Carlos,
Tulipán s/n, Mostoles, 28933, Madrid, Spain

Marco A. Fontelos

Instituto de Ciencias Matemáticas (ICMAT, CSIC-UAM-UC3M-
UCM), C/ Nicolás Cabrera 15, 28049 Madrid, Spain.

Manuel Arrayás

Área de Electromagnetismo, Universidad Rey Juan Carlos,
Tulipán s/n, Móstoles, 28933, Madrid, Spain

August 26, 2025

Abstract

We develop and implement numerically a phase field model for the growth and detachment of a gas bubble resting on an electrode and being filled with hydrogen produced by water electrolysis. The bubble is surrounded by a viscous liquid, has a prescribed static contact angle and is also subject to gravitational forces. We compute, as a function of the static contact angle, the time at which the bubble detaches from the substrate and what volume it has at that time. We also investigate the dependence of the detachment time on other parameters such as the applied voltage and the hydrogen ion concentration at the fluid bulk.

1 Introduction

The study of the nucleation, growth and detachment of gas bubbles inside viscous liquids has relevance across a wide range of applications including boiling (cf. [17]), cavitation (cf. [14]), microfluidics (cf. [13]), and electrochemical systems (cf. [12]). In the electrochemical context, gas bubbles form at electrodes as a result of chemical reactions, such as the hydrogen generation during water electrolysis, a process of growing industrial importance for sustainable energy storage and conversion (see for instance [20]). Hence, the search for methods and techniques to optimize the energy production (cf. [15]) becomes of special interest.

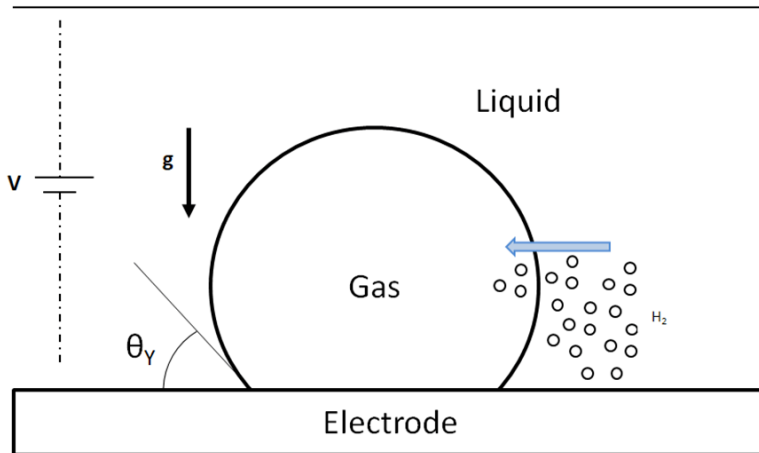


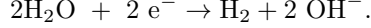
Figure 1: Sketch of physical settings: H_2 is produced at the electrode by water electrolysis using the electrons e^- provided by the battery, and diffuses inside the bubble with the contact angle θ_Y . The bubble will grow and detach once buoyancy forces due to gravity overcome the surface tension forces that attach the bubble to the surface.

In our previous work [1], we have investigated the dynamics of bubble detachment under different external conditions using a phase field approach (for a general description of the method see [5], [6], for its application for fluid mechanical problems [7], [8], [10], [9], [11] and for the implementation in a problem for bubble detachment [21]). This method, which replaces sharp interfaces with smoothly varying diffuse interfaces, allowed us to effectively model the complex interfacial dynamics and topological changes associated with bubble evolution. We focused on the interplay between buoyancy, surface tension, and hydrodynamic forces in determining the detachment behaviour of bubbles, providing insights into the physical mechanisms governing gas release in electrochemical systems.

In the present study, we extend this framework by incorporating the effects of electrochemical reaction kinetics and electric fields. These additions are essential for a more comprehensive understanding of bubble dynamics in realistic electrolysis environments, where the local gas production rate and the electric field distribution significantly influence bubble growth and detachment. By coupling the phase field model with reaction-diffusion equations and electrostatic interactions, we aim to capture the feedback between electrochemical activity and fluid dynamics, offering a more complete picture of gas evolution

at electrodes.

The bubble grows due to the influx of hydrogen molecules (H_2) that is produced through a water electrolysis process at the cathode:



In figure 1, we provided a sketch of the physical situation to be considered in this work. The phase field model coupled with Navier-Stokes equation which we used in our previous work [1] must be extended in order to incorporate the electrochemistry processes. Sections 2, 3, and 4 are dedicated to the development of this extended model. In Section 2, we introduce the modelling of electrochemical phenomena and the motion of the involved fluids. In section 3 some dimensionless parameters are introduced, along with their corresponding physical values. Section 4 focuses on incorporating the phase-field formulation into the previously established equations in order to develop a complete diffuse interface model to be implemented numerically. Section 5 contains the numerical simulations of the model. In particular, we investigate the influence of the contact angle on the detachment time and gas bubble volume, as well as the effect of the applied electrode potential on the overall process. The paper concludes with a summary of our findings and prospects for future work.

2 Mathematical model

In this section we will develop a mathematical model for the production of hydrogen at an electrolytic device and the growth of a bubble filled by gaseous hydrogen. The model will entail essentially two parts: 1) the motion of the fluids involved, which will typically be water and gaseous hydrogen, 2) the production and flux of hydrogen molecules from the reaction at the electrode, as well as hydrogen ions (protons).

2.1 Fluid equations

Both the external flow and the growing bubble are fluids. In the first case we typically consider water and, in the second, gaseous hydrogen. The velocities involved are small in comparison with the sound velocity so that we will neglect compressibility effects of the gas inside the bubble and will merely treat it as an incompressible fluid. Hence, denoting ρ_i , $i = 1, 2$ the densities of both fluids, the velocity field will satisfy Navier-Stokes equations:

$$\frac{\partial(\rho_i \mathbf{v})}{\partial t} + \rho_i \mathbf{v} \cdot \nabla \mathbf{v} - \nabla \cdot \mathbf{S}_i = -\nabla p - \rho_i g \mathbf{e}_z, \quad (1)$$

$$\nabla \cdot \mathbf{v} = 0, \quad (2)$$

with a viscous stress

$$\mathbf{S}_i = \frac{\eta_i}{2} (\nabla \mathbf{v} + \nabla \mathbf{v}^T) \quad (3)$$

where η_i , $i = 1, 2$ are the viscosities of both fluids, and the balance of force condition at the interface:

$$(-p\mathbf{I} + \mathbf{S}_i) \cdot \mathbf{n} = \sigma \kappa \mathbf{n} \quad (4)$$

where $\kappa(\mathbf{x}, t)$ is the mean curvature at any point \mathbf{x} at the surface of the bubble in contact with the liquid. We consider, as initial data, a bubble consisting of a truncated sphere with radius R .

The introduction of a characteristic velocity U defined from the following balance between inertial and gravitational forces

$$\rho_1 \frac{U^2}{R} = \rho_1 g,$$

allows to write the system in terms of the following dimensionless numbers

$$Bo = \frac{gR^2\rho_1}{\sigma}, \quad Re = \frac{UR\rho_1}{\mu}, \quad (5)$$

where Bo is the Bond number and Re the Reynolds number in the liquid phase (ρ_1), as well as the density and viscosity ratios

$$\gamma = \frac{\rho_2}{\rho_1}, \quad \chi = \frac{\eta_2}{\eta_1}. \quad (6)$$

Hence, the velocity field satisfies

$$\frac{\partial \mathbf{v}}{\partial t} + \mathbf{v} \cdot \nabla \mathbf{v} - \frac{1}{Re} \Delta \mathbf{v} = -\nabla p - Bo \mathbf{e}_z, \quad \text{in the liquid phase,} \quad (7)$$

$$\frac{\partial \mathbf{v}}{\partial t} + \mathbf{v} \cdot \nabla \mathbf{v} - \frac{\chi}{Re} \Delta \mathbf{v} = -\nabla p - \gamma Bo \mathbf{e}_z, \quad \text{in the gas phase.} \quad (8)$$

2.2 Electrochemistry equations and 1D stationary solutions

The concentration n of protons (H^+), n_{H_2} of H_2 and the electric potential φ satisfy under stationary conditions in the bulk

$$\Delta n = 0, \quad (9)$$

$$\Delta n_{\text{H}_2} = 0, \quad (10)$$

$$\nabla \cdot (n \nabla \varphi) = 0. \quad (11)$$

Far from the cathode, at $z = L$, we can take some reference values,

$$n = n_r, \quad n_{\text{H}_2} = n_{\text{H}_{2r}}, \quad \varphi = V, \quad \text{at } z = L. \quad (12)$$

At the cathode ($z = 0$) we have the following conditions in the region of the electrode surface not covered by bubbles,

$$\frac{\partial n}{\partial z} = \frac{1}{D_+} \omega, \quad (13)$$

$$\frac{\partial n_{\text{H}_2}}{\partial z} = -\frac{1}{D_{\text{H}_2}} \omega, \quad (14)$$

$$\frac{F}{RT} \frac{\partial \varphi}{\partial z} = \frac{1}{n} \omega, \quad (15)$$

where the reaction rate ω satisfies the Butler-Volmer equation

$$\omega = \frac{i_0}{2F} \left(e^{\frac{2\alpha F}{RT}(\varphi - \varphi_r)} \left(\frac{n}{n^s} \right)^2 - e^{-\frac{2(1-\alpha)F}{RT}(\varphi - \varphi_r)} \frac{n_{\text{H}_2}}{n^s} \right), \quad (16)$$

with n^s is some reference concentration (say 1 mol/l for instance) and φ_r is some reference potential. Here ω is the amount of protons produced per unit time and unit area. R , F and T are the universal gas constant, the Faraday constant and the temperature respectively. The transfer coefficient α is a model constant, while i_0 is the exchange current in the standard reference state, which is a function of the material and structure of the electrode. The conditions (13)-(15) express the balance of the flux of each electro active species entering or leaving the double layer – formed at the cathode – by diffusion and migration from the bulk. In equations (13) and (14), D_+ and D_{H_2} are the diffusivity of protons and dissolved hydrogen respectively. The electric field at the boundary layer is given by (15) (further details of the model can be found in [2]).

We have the following 1D solution for the system (9)-(11),

$$\begin{aligned} \frac{\partial \varphi}{\partial z} &= \frac{K}{n(z)}, \\ n(z) &= A + Bz, \\ n_{\text{H}_2}(z) &= C + Dz, \end{aligned}$$

and hence

$$\varphi(z) = \frac{K}{B} \log(A + Bz) + E, \quad (17)$$

where K, A, B, C, D and E are constants to be determined from boundary conditions. The conditions (12) at $z = L$ yield,

$$V = \frac{K}{B} \log(A + BL) + E, \quad (18)$$

$$n_{\text{H}_2r} = C + DL, \quad (19)$$

$$n_r = A + BL. \quad (20)$$

On the other hand, from the boundary conditions at the electrode we have

$$-D_{\text{H}_2} D = \omega, \quad (21)$$

$$B = \frac{1}{D_+} \omega, \quad (22)$$

$$\frac{F}{RT} \frac{K}{A} = \frac{1}{AD_+} \omega. \quad (23)$$

Solving the system we get

$$D = -\frac{1}{D_{\text{H}_2}} \omega, \quad (24)$$

$$C = n_{\text{H}_{2r}} + \frac{L}{D_{\text{H}_2}} \omega, \quad (25)$$

$$B = \frac{1}{D_+} \omega, \quad (26)$$

$$A = n_r - \frac{L}{D_+} \omega, \quad (27)$$

$$K = \left(\frac{F}{RT} \right)^{-1} \frac{1}{D_+} \omega, \quad (28)$$

$$E = \left(\frac{F}{RT} \right)^{-1} \log n_r - V, \quad (29)$$

all in terms of the reaction rate at the electrode ω . We can then introduce in the Butler-Volmer equation the concentrations and potential as functions of ω and obtain an algebraic equation for ω . In fact, we can find an equilibrium (no production of hydrogen) when

$$e^{-2 \frac{F}{RT} (\varphi_r - \varphi_{eq})} = \frac{n_r^2}{n_{\text{H}_{2r}}}. \quad (30)$$

Then one has, as a function of the value of the potential at the electrode φ

$$\omega = \frac{i_0}{2F} \left[\left(\frac{n_r^2}{n_{\text{H}_{2r}}} \right)^{-\alpha} e^{\frac{2\alpha F}{RT} (\varphi - \varphi_r)} n^2 - e^{-\frac{2(1-\alpha)F}{RT} (\varphi - \varphi_r)} \left(\frac{n_r^2}{n_{\text{H}_{2r}}} \right)^{1-\alpha} n_{\text{H}_2} \right], \quad (31)$$

and since

$$\varphi(0) - \varphi_r = \frac{K}{B} \log A + E = V + \left(\frac{F}{RT} \right)^{-1} \log \left(1 - \frac{L}{n_r D_+} \omega \right),$$

$$n(0) = A = n_r - \frac{L}{D_+} \omega,$$

$$n_{\text{H}_2}(0) = C = n_{\text{H}_{2r}} + \frac{L}{D_{\text{H}_2}} \omega,$$

we obtain the following relations for small deviations from the equilibrium $\delta\varphi, \delta\omega, \delta V$:

$$\delta\varphi = \delta V - \left(\frac{F}{RT}\right)^{-1} \frac{L}{n_r D_+} \delta\omega, \quad (32)$$

$$\begin{aligned} \delta\omega = & \frac{i_0}{2F} \left[\frac{2F}{RT} \left(\frac{n_r^2}{n_{H_{2r}}}\right)^{1-\alpha} n_{H_{2r}} \right] \delta\varphi \\ & + \frac{i_0}{2F} \left[\left(\frac{n_r^2}{n_{H_{2r}}}\right)^{-\alpha} 2n_r \left(-\frac{L}{D_+} \delta\omega\right) - \left(\frac{n_r^2}{n_{H_{2r}}}\right)^{1-\alpha} \frac{L}{D_{H_2}} \delta\omega \right], \end{aligned} \quad (33)$$

leading to

$$\delta V = \frac{1 + \frac{i_0}{F} \frac{2L}{D_+} \left(\frac{n_r^2}{n_{H_{2r}}}\right)^{1-\alpha} \frac{n_{H_{2r}}}{n_r} + \frac{i_0}{2F} \left(\frac{n_r^2}{n_{H_{2r}}}\right)^{1-\alpha} \frac{L}{D_{H_2}}}{\frac{i_0}{2F} \left(\frac{2F}{RT} \left(\frac{n_r^2}{n_{H_{2r}}}\right)^{1-\alpha} n_{H_{2r}}\right)} \delta\omega, \quad (34)$$

which yields a linear relation between the reaction rate $\delta\omega$ and the variations in the applied over potential δV . Note that prefactor of $\delta\omega$ in (34) is positive, so that an increment in the potential corresponds to an increment on the reaction rate.

2.3 Bubble H_2 influx

The influx of H_2 that fills the bubble is given by

$$J = - \int_{\partial\Omega} D_{H_2} \nabla n_{H_2} \cdot \mathbf{n} dS, \quad (35)$$

where $\partial\Omega$ is the part of the surface of the bubble that is in contact with the surrounding liquid. If we assume that the temperature T remains constant, the concentration of H_2 is constant throughout the bubble and the gas satisfies the law of perfect gases. We have then for a given mass m of H_2

$$pV = n_{H_2} RT = \frac{m}{m_{H_2}} RT, \quad (36)$$

being m_{H_2} the H_2 molecular mass, which allows to compute the volume of the bubble at any given time knowing the pressure and the mass m . Taking time derivatives we deduce

$$\frac{dp}{dt} V + p \frac{dV}{dt} = \frac{RT}{m_{H_2}} \frac{dm}{dt},$$

so the change in the volume is

$$\frac{dV}{dt} = \frac{RT}{m_{H_2} p} \left(\frac{dm}{dt} - m \frac{d \log p}{dt} \right). \quad (37)$$

Using (35), the total mass can be computed at any time since

$$\frac{dm}{dt} = m_{\text{H}_2} J. \quad (38)$$

The pressure p can be found by solving the hydrodynamic equations. Nevertheless, we can safely assume the term involving dp/dt to be small compared with other terms since the pressure inside the bubble, for a bubble which grows slowly, is determined from the balance between jump in pressure across the interface and surface tension (i.e. the inverse of the bubble radius) and this changes slowly in time. Hence, the change in volume will be determined from the change in the total mass of H_2 inside the bubble.

3 Physical parameters and scales

In this section we discuss the typical values of the physical parameters involved in the problem. Firstly, concerning the fluid parameters (for water and H_2) we have at 298 K and 1 atm,

$$\begin{aligned} \rho_1 &= 10^3 \text{ kg/m}^3, \\ \rho_2 &= 0.08988 \text{ kg/m}^3, \\ \mu_1 &= 0.89 \cdot 10^{-3} \text{ Pa} \cdot \text{s}, \\ \mu_2 &= 8.874 \cdot 10^{-5} \text{ Pa} \cdot \text{s}, \\ \sigma &= 72.8 \cdot 10^{-3} \text{ N/m}. \end{aligned} \quad (39)$$

Secondly, we note that, at 298 K and 1 atm,

$$\frac{F}{RT} = \frac{96500 \text{ C/mol}}{(8.314 \text{ J/(mol K)}) \cdot (298 \text{ K})} = 38.95 \text{ V}^{-1}.$$

We can also introduce the dimensionless number

$$\iota = \frac{i_0 L}{FD_{\text{H}_2} n_s} = 0.83, \quad (40)$$

by taking for instance $L = 0.01 \text{ m}$ and $i_0 = 10^{-2} \text{ A/m}^2$, and using (39). In addition, the diffusivity of hydrogen and H^+ in water are

$$D_{\text{H}_2} = 1.6 \times 10^{-9} \text{ m}^2/\text{s}, \quad (41)$$

$$D_+ = 9.3 \times 10^{-9} \text{ m}^2/\text{s}, \quad (42)$$

respectively, and we can define the diffusivity ratio as

$$\delta = \frac{D_{\text{H}_2}}{D_+} = \frac{1.6}{9.31} = 0.17. \quad (43)$$

Next we rescale the concentrations with the saturation concentration for H_2

$$n_s = 7.8 \times 10^{-4} \text{ mol/l}, \quad (44)$$

so that we make concentrations dimensionless and rescale the potential with $(\frac{F}{RT})^{-1}$ to make it dimensionless. We rescale space with the length L and finally get the rescaled boundary conditions,

$$\frac{\partial \varphi}{\partial z} = \frac{1}{n} \delta \omega \quad (45)$$

$$\frac{\partial n}{\partial z} = \delta \omega \quad (46)$$

$$\frac{\partial n_{\text{H}_2}}{\partial z} = -\omega \quad (47)$$

at the electrode. Similarly

$$n = n_r, \quad n_{\text{H}_2} = n_{\text{H}_{2r}}, \quad \varphi = V \quad \text{at } z = 1 \quad (48)$$

The Butler-Volmer equation is then

$$\omega = \frac{\iota}{2} \left(e^{2\alpha(\varphi - \varphi_{eq})} n^2 - e^{-2(1-\alpha)(\varphi - \varphi_{eq})} n_{\text{H}_2} \right). \quad (49)$$

Note that $\omega = 0$ (no reaction) when $\varphi = \varphi_0$ with

$$\varphi_0 - \varphi_{eq} = \frac{1}{2} \log \frac{n^2(z=0)}{n_{\text{H}_2}(z=0)},$$

and since $n = n_r$, $n_{\text{H}_2} = n_{\text{H}_{2r}}$, $V = \varphi_0$ in that case we have

$$\varphi_0 - \varphi_{eq} = \frac{1}{2} \log \frac{n_r^2}{n_{\text{H}_{2r}}}.$$

If we take $V > \varphi_0$ then $n_{\text{H}_2}(z) \geq n_{\text{H}_{2r}}$, $n(z) \leq n_r$. We will typically take $n_{\text{H}_{2r}} = 1$ close to saturation so that the bulk is over saturated, $n > 1$ (so that the concentration of H^+ is larger than the saturation concentration which is under standard conditions $7.8 \cdot 10^{-4}$ mol/l that would represent a pH of 3.1).

4 Phase field modelling

One of the most effective methods to study multiphase flows is the so-called phase field method. The main idea is to replace sharp interfaces by “diffuse” interfaces where a phase field function $\phi(\mathbf{x}, t)$ experiences sharp transitions (across the diffuse interface with a thickness of order ε sufficiently small) between to limiting values (say $\phi = 1$ and $\phi = -1$, for instance) corresponding to two different fluids. One of the main advantages of introducing diffuse interfaces is their ability to naturally handle topological changes in fluid domains. One needs to provide a suitable PDE to the phase field $\phi(\mathbf{x}, t)$ and couple to other fluid variables in a proper way. This has been studied in many papers (cf. [7], [8], [10], [9], [11] for instance). For the phase field function, the suitable equation is a fourth order PDE called the Cahn-Hilliard equation (firstly introduced in

[4], see also [3]) including a convection term with a velocity $\mathbf{v}(\mathbf{x}, t)$ which is the fluid velocity:

$$\frac{\partial \phi}{\partial t} + \mathbf{v} \cdot \nabla \phi = \nabla \cdot (M \nabla \mu), \quad (50)$$

with

$$\mu = -\varepsilon \Delta \phi + \frac{1}{\varepsilon} W'(\phi), \quad (51)$$

where μ is the so-called chemical potential.

In (50) M is a “mobility” factor and in (51) $W(\phi)$ is a phase-field potential with the property of having two local minima at values of ϕ corresponding to the two phases. In particular we will take $W(\phi) = \phi^2(1 - \phi^2)$.

4.1 Navier-Stokes

Concerning Navier-Stokes system, we introduce the phase field as

$$\frac{\partial(\rho(\phi) \mathbf{v})}{\partial t} + \rho(\phi) \mathbf{v} \cdot \nabla \mathbf{v} - \nabla \cdot \mathbf{S} = -\nabla p + \mu \nabla \phi - \rho(\phi) g \mathbf{e}_z, \quad (52)$$

where the viscous stress tensor is given by

$$\mathbf{S} = \frac{\eta(\phi)}{2} (\nabla \mathbf{v} + \nabla \mathbf{v}^T), \quad (53)$$

and the material parameters $\rho(\phi)$ and $\eta(\phi)$ interpolate between the fluids densities and viscosities respectively:

$$\rho(\phi) = \rho_1 \phi + \rho_2 (1 - \phi), \quad (54)$$

$$\eta(\phi) = \eta_1 \phi + \eta_2 (1 - \phi). \quad (55)$$

We will also assume fluid incompressibility:

$$\nabla \cdot \mathbf{v} = 0, \quad (56)$$

and for the phase field the boundary condition

$$\frac{\partial \mu}{\partial n} = 0, \quad (57)$$

denoting the change of the chemical potential in the normal direction. The condition (57) is not sufficient for a fourth order equation such as (50) and we need another boundary condition. Following [9] and [10], we will impose the condition

$$\sigma_0 \varepsilon \frac{\partial \phi}{\partial n} = \sigma'_{fs}(\phi), \quad (58)$$

where $\sigma'_{fs}(\phi)$ interpolates between the liquid/solid interfacial energy σ_{LS} and the gas/solid interfacial energy σ_{GS} :

$$\sigma_{fs}(\phi) = \frac{\sigma_{GS} + \sigma_{LS}}{2} + \frac{\sigma_{GS} - \sigma_{LS}}{2} \sin\left(\frac{\pi \phi}{2}\right), \quad (59)$$

and σ_0 is proportional to the liquid/gas interfacial energy σ_{LG} :

$$\sigma_0 = \frac{3\sqrt{2}}{8}\sigma_{LG}. \quad (60)$$

In this way, the condition (58) imposes, in the limit $\varepsilon \rightarrow 0$, a liquid/gas contact (or Young's) angle θ_Y such that

$$\cos \theta_Y = \frac{\sigma_{GS} - \sigma_{LS}}{\sigma_{GS}}. \quad (61)$$

4.2 Electrochemistry

We introduce the phase field into the equations for the concentration of H_2 by writing the diffusion coefficient as a function of the phase field ϕ :

$$D_1(\phi) = D_{H_2} \frac{1 + \phi}{2}. \quad (62)$$

We impose $n_{H_2} = n_s$ at the surface of the bubble by introducing a penalization term $C_b (n_s - n_{H_2})$ with $C_b \gg 1$ so that $n_{H_2} \simeq n_s$ inside the bubble and hence at its boundary. The resulting equation is

$$\nabla \cdot (D_1(\phi) \nabla n_{H_2}) + C_b (n_s - n_{H_2}) = 0. \quad (63)$$

Analogously, for the concentration of H^+ and the electrostatic potential we write the equations

$$D_2(\phi) = D_{H^+} \frac{1 + \phi}{2}, \quad \nabla \cdot (D_2(\phi) \nabla n) = 0, \quad (64)$$

and

$$\nabla \cdot (n \nabla \varphi) = 0, \quad (65)$$

respectively. Finally, the reaction rate at the electrode is corrected in such a way that no reaction takes place at the part of the electrode covered by the bubble:

$$\omega_\phi = \frac{1 + \phi}{2} \omega. \quad (66)$$

Thus the conditions at the reacting electrode are

$$\frac{\partial n}{\partial z} = \frac{1}{D_+} \omega_\phi, \quad (67)$$

$$\frac{\partial n_{H_2}}{\partial z} = -\frac{1}{D_{H_2}} \omega_\phi, \quad (68)$$

$$\frac{F}{RT} \frac{\partial \varphi}{\partial z} = \frac{1}{n} \omega_\phi, \quad (69)$$

and the conditions at $z = L$ remain unchanged:

$$n = n_r, \quad n_{H_2} = n_{H_{2r}}, \quad \varphi = V. \quad (70)$$

4.3 Bubble H_2 influx

We determine the mass influx by performing a balance of mass analysis between the mass of H_2 produced at the electrode, the mass lost across the domain's boundaries and the change of the mass of H_2 at the liquid bulk. In this way, we determine the amount of gas that enters the bubble and change its volume accordingly. We inject the corresponding amount of mass per unit time as a source inside the bubble. The flow inside the bubble diffuses the incoming gas very quickly so that we keep the gas density constant through the whole bubble except for a small neighbourhood around the source.

5 Numerical results

We will use the phase field model developed in the previous sections to simulate the behaviour of a growing bubble under various physical conditions. First we will study the effect of the contact angle on time of detachment and the volume of gas detached with the bubble. Secondly, we will see how the magnitude of the applied potential V influences the gas production.

The simulations have been carried out using the Comsol PDE software [22]. The mathematical models previously proposed have been introduced and solved using a finite element scheme, coupling the different physics through a semi-discrete time approach. This approach divides the governing equations into the time-independent (diffusion and potential) and the time-dependent equations (phase field model and Navier Stokes, NS from now on, equations) in such a way that the time domain is subdivided into n distinct intervals of 0.1 s duration each, between which the diffusion physics of n_{H_2} , n_p and the potential are recalculated. Therefore, at each time period of 0.1 s, the phase field and velocity field of the NS equations are solved, using stationary values (calculated previously) of the concentrations and potential during this time. After this time, the values of the concentrations are recalculated taking into account the values of the phase field obtained in the last instant of time calculated in the previous step.

In our simulations we use a cylindrical system of coordinates and we will assume axial symmetry with the origin placed in the electrode plane, being z and r the vertical and radial coordinates respectively. The simulation domain consists of a cylinder supported at $z=0$, with 3 cm radius and 1 cm height (simulating an electrolysis cell with a circular electrode of 6 cm diameter and 1 cm height). The bubble is located at the centre of the cell (axis of symmetry), initially consisting of a truncated sphere of 1 mm radius resting on the electrode with 3/4 of its diameter protruding, which corresponds to an initial contact angle of 60° with the electrode (plane $z=0$).

Initially the simulation domain is divided into two parts, inside and outside the bubble. The initial values of the phase field are set to -1 and 1 at the interior of the bubble and the surrounding fluid respectively, while the NS equations assume steady flow initial conditions ($\mathbf{v} = 0$) in the whole domain. The station-

ary versions of the diffusion equations are solved iteratively using the following initial conditions: the H_2 concentration is set to the value $n_{\text{H}_2, \text{in}} = n_s = 1 \text{ mol/l}$ (inside the bubble) and $n_{\text{H}_2, \text{out}} = n_{\text{H}_2, r} = 1 \text{ mol/l}$ (outside the bubble). Also as initial conditions, we assume that there is no proton concentration inside the bubble ($n_{p, \text{in}} = 0 \text{ mol/l}$) and that the concentration outside the bubble has a value $n_{p, \text{out}} = n_s \text{ mol/l}$. Finally, the potential is set to 0 V in the whole domain. At each time step, we solve the stationary versions of the diffusion equations using the values of the previous step. The same approach is followed for the potential.

For the boundary conditions, non-slip walls ($v_r = 0$) have been used on the contact surfaces of the cell, in which it has been further assumed that the equilibrium contact angle between the gas and liquid phase is θ_Y through the following relation:

$$\mathbf{n} \cdot \nabla \phi = \cos \theta_Y |\nabla \phi|, \quad (71)$$

where \mathbf{n} refers to the surface normal vector pointing outside the domain.

In the diffusion equations it is further assumed that the side walls of the cell do not diffuse the substances ($\mathbf{n} \cdot \nabla n_{\text{H}_2} = 0$; $\mathbf{n} \cdot \nabla n_p = 0$) and the following Dirichlet boundary conditions are applied: the concentration of H_2 is set to the saturation value on the top surface ($n_{\text{H}_2, \text{top}}$) of the cell, while the concentration of protons is set to a variable value ($n_{p, \text{top}}$). The potential at the top wall is set to $V_{\text{top}} = V_0 + V$, where V is a controlling variable and V_0 is calculated using the following relation:

$$V_0 = \log(n_{p, \text{top}}^2 / n_{\text{H}_2, \text{top}}). \quad (72)$$

In addition, the following boundary conditions for the diffusion equations are imposed on the electrode (except the part where the bubble contacts the surface), for the hydrogen equation:

$$\mathbf{n} \cdot \nabla n_{\text{H}_2} = \omega, \quad (73)$$

being ω the Butler-Volmer constant. The proton equations flux is set to:

$$\mathbf{n} \cdot \nabla n_p = -\omega \delta, \quad (74)$$

where δ is the diffusivity ratio (0.17 in these simulations). Finally the flux imposed in the potential equation is:

$$n_p \mathbf{n} \cdot \nabla V = \frac{\partial n_{\text{H}_2}}{\partial z}. \quad (75)$$

Finally, the hydrogen production is simulated by injecting a net mass flux into the bubble during the time-dependent analysis, where this flux is calculated in the following way:

$$J = 1.24 \times 10^{-10} \cdot \int_{\text{electrode}} \frac{\partial n_{\text{H}_2}}{\partial z} dr. \quad (76)$$

Lastly, material properties are included for NS physics, setting the dynamic viscosity of water in $\eta_w = 0.001 \text{ Pa} \cdot \text{s}$ and its density in $\rho_w = 1000 \text{ kg/m}^3$. The viscosity and density of hydrogen are $\eta_{H_2} = 0.00084 \text{ Pa} \cdot \text{s}$ and $\rho_{H_2} = 0.089 \text{ kg/m}^3$ respectively, where one may notice that hydrogen viscosity is slightly greater than the real value, which was increased in order to guarantee a smooth dispersion of the injected gas and to avoid undesirable side effects, such as excessive phase field distortion produced by vortices in the bubble. The whole domain is meshed using equally-sized triangular elements of linear shape functions with a maximum element length of 0.01 mm, which gives an average element number of 120000.

Figure 2 shows a simulation with the previously mentioned parameters for a case where the contact angle is $\pi/2$, the voltage applied is $V = 5 \text{ V}$ and the proton concentration at the top surface is $n_{p,top} = 2 \text{ mol/l}$.

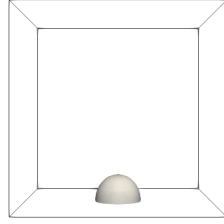
The figure shows four stages in the evolution of the bubble growth, from left to right and top to bottom. At the instant 0.1 s is shown how the angle relaxes from the initial value $\pi/3$ to the equilibrium value θ_Y . The second plot shows the time at $t = 2.06 \text{ s}$, where the bubble has grown considerably. The two last images correspond to the moments right before ($t = 2.10 \text{ s}$) and immediately after ($t = 2.11 \text{ s}$) of the detachment and lift-off. Note that a small amount of gas has been left on the electrode as a remnant.

An example of hydrogen concentration distribution during the simulations is shown in figure 3. Specifically, the upper part of the figure illustrates the hydrogen concentration for a case with an equilibrium contact angle of $\theta_Y = \pi/2$, at a time step prior to bubble lift-off. It is worth noting that the initial contact angle in the simulations is always $\pi/3$ and relaxes to the equilibrium angle during the initial stages steps of the simulations. The lower part of the figure depicts the hydrogen flux (i.e. the derivative of the hydrogen concentration n_{H_2} with respect to the vertical coordinate z) generated at the electrode and calculated from the corresponding diffusion map. This variation is directly related to the mass flux injected at each time step, as described by equation (76).

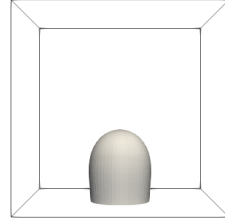
As expected, the maximum concentration appears in the neighbourhood of the electrode where the production takes place. The geometry in the neighbourhood of the contact line is that of a 2D wedge of angle θ_Y . The value of n_{H_2} experiences a jump from its value at the side of the wedge that corresponds to the electrode to n_s at the drop side of the wedge. This implies that a singularity in the gradient of n_{H_2} must develop as we can see in the lower graph in Figure 3. Hence, an important part of the production of H_2 takes place in the neighbourhood of the contact line since $\omega = -\partial n_{H_2}/\partial z$ is singular there.

5.1 The effect of contact angle

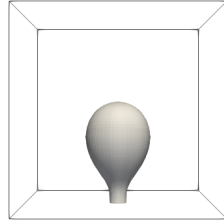
We address next the dependence of the gas production on the contact angle θ_Y . The size of the bubble when it detaches from the substrate depends strongly on θ_Y as we can see in figure 4. For the set of parameters in our simulation, the volume changes a full order of magnitude from $\theta_Y = 60^\circ$ to $\theta_Y = 110^\circ$. The smallest bubble, corresponding to $\theta_Y = 60^\circ$, has a volume of 10 mm^3 (i.e. a



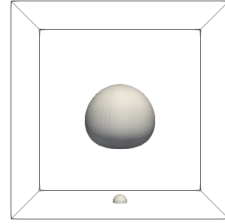
(a) $t = 0.1 \text{ s}$



(b) $t = 1.5 \text{ s}$

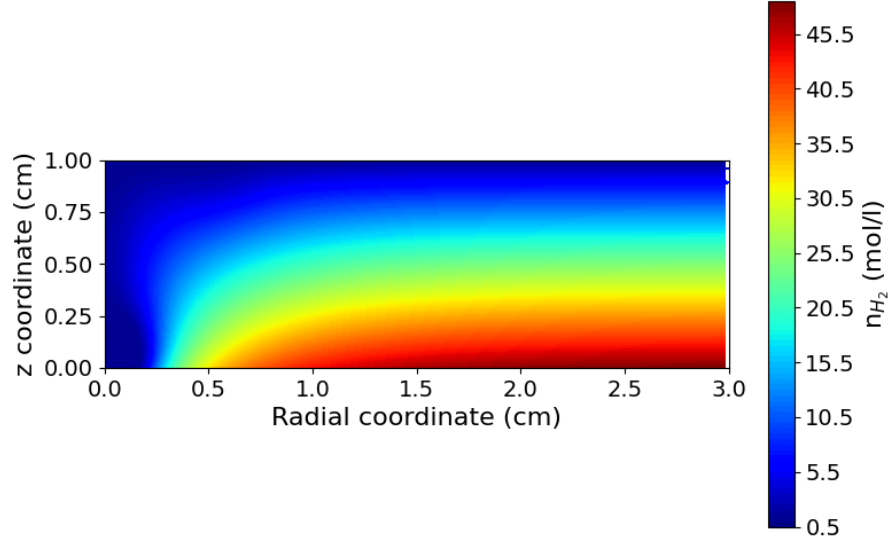


(c) $t = 1.72 \text{ s}$

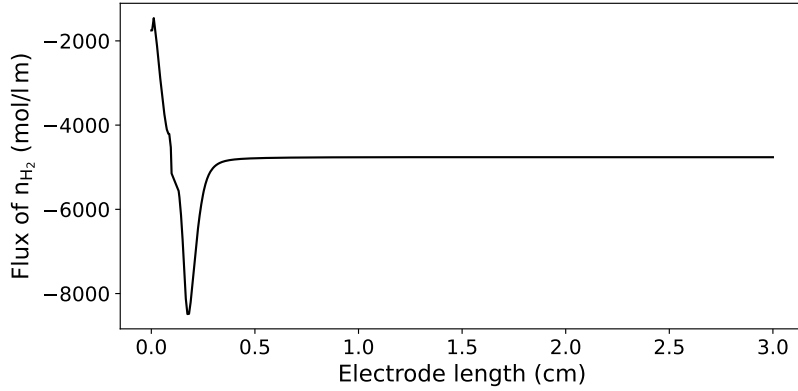


(d) $t = 1.73 \text{ s}$

Figure 2: Bubble growth evolution stages for a $\pi/2$ contact angle simulation, an applied voltage $V = 5 \text{ V}$ and the proton concentration at the top surface $n_{p,top} = 2 \text{ mol/l}$. The figure shows four stages in the bubble growth. The top-left image shows the initial relaxation to the equilibrium contact angle, while the top right figure shows an intermediate instant where the sphere has grown substantially. The bottom figures shows the instants before and after the lift off, where it may be appreciated the remanent stuck at the electrode produced if the contact angle is great enough.



(a) Hydrogen concentration distribution



(b) Hydrogen generation in the electrode

Figure 3: Hydrogen generation and distribution at time $t = 1$ s prior to bubble lift-off. The top figure (a) presents the distribution map of hydrogen concentration within the cell. The bottom figure (b) displays the spatial derivative of hydrogen concentration with respect to z (vertical flux), calculated along the electrode.

radius of 1.33 mm) and the largest, corresponding to $\theta_Y = 110^\circ$, has a volume of 45.9 mm³ (i.e. a radius of 2.2 mm). On the other hand, we can evaluate the time to detachment and add the estimated time that would take a nucleating bubble to develop into our initial data in order to estimate the full time that takes for a bubble to grow up to detachment as a function of θ_Y . We represent these times in figure 5. The time spans from $t = 0.7$ s for $\theta_Y = 60^\circ$ up to $t = 2.7$ s for $\theta_Y = 110^\circ$. Bubbles with $\theta_Y = 0$ would detach immediately after nucleation with zero volume while bubbles with θ_Y close to 180° would take an exceedingly long time to detach. Both of the graphs seem to indicate a linear relationship between the volume of gas produced and the time taken for bubble detachment with respect to the contact angle. Therefore, no optimal angle that maximizes the volume-time ratio can be derived from this analysis. However, it should be emphasized that the volume shown in the graph represents the entire hydrogen gas present in the simulation cell at the moment of lift off, including the remnant that remains attached to the electrode above a certain contact angle ($\theta_Y > 83^\circ$). This remainder can serve as a nucleating core for new bubble growth, speeding up the reaction.

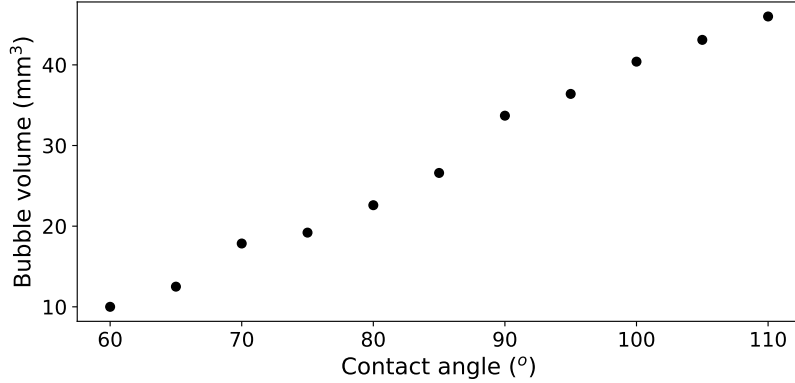


Figure 4: Bubble volume at lift-off instant for different contact angles. Each point in the graph corresponds to a single simulation where only the contact angle varies.

5.2 Modifying voltage and acidity

The two remaining control parameters of the mathematical model presented are the applied voltage at the electrode and the acidity of the medium, which we control by setting the concentration of protons on the top wall of the domain. In this section, we present the most relevant results of this analysis, which can be seen in figure 6, where it is shown how the bubble lift-off time decays with the applied voltage, for different values of the proton concentration. Regarding the latter, it can be seen how the time decay tends to be more pronounced when

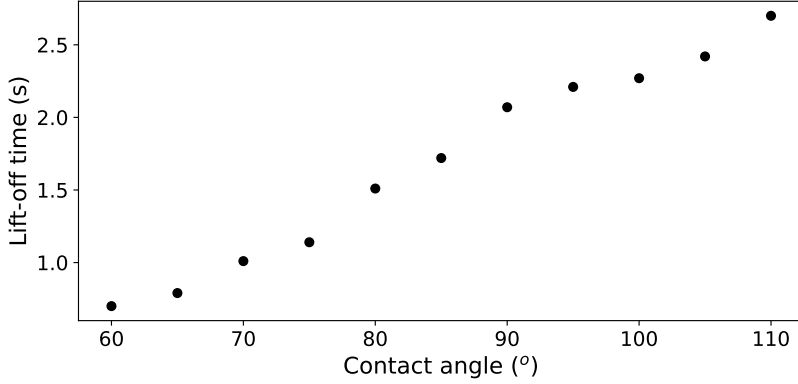


Figure 5: Time to lift-off for different contact angles. Each point in the graph corresponds to a single simulation where only the contact varies. Overall time is represented in the horizontal axis, which takes into account the coalescence time plus the simulation time from the initial conditions until the moment when the bubbles lift-off. The coalescence time has been assumed calculating the growth rate in the first instants and extrapolating this trend backwards.

the acidity of the medium is lower (lower concentration of protons in the upper wall) and remains almost unchanged when the acidity increases. In this figure, the time spans from $t = 0.69$ s for $V = 15$ V and $n_{p,top} = 5$ to $t = 3.35$ s for $V = 5$ V and $n_{p,top} = 1$. We remark that in all cases a significant increase in the potential does not translate into an equivalent decrease in the detachment time and hence into the hydrogen production. This effect of the applied voltage is even smaller for more acidic media.

6 Conclusions

We have studied the growth and detachment of a gaseous bubble in a water electrolyzer. Hydrogen is produced through chemical reactions at an electrode and transported by diffusion into a bubble producing its growth and eventual detachment from the substrate (the electrode). The model consists of fluid mechanical equations (Navier-Stokes) for both the gas inside the bubble and the surrounding fluid, together with classical drift-diffusion equations for the chemical species, i.e. hydrogen molecules and hydrogen ions (protons). The model is completed with an equation for the electric inside the liquid medium. Appropriate boundary conditions have also been introduced, some of them involving the reaction rate at the electrode for the chemical reaction producing H_2 from H^+ . This reaction rate follows the Butler-Volmer equation.

The above model, as such, is very difficult to solve when sharp moving interfaces (between the bubble and the medium) and contact lines are involved. In order to overcome this difficulty we introduce a phase field formulation of

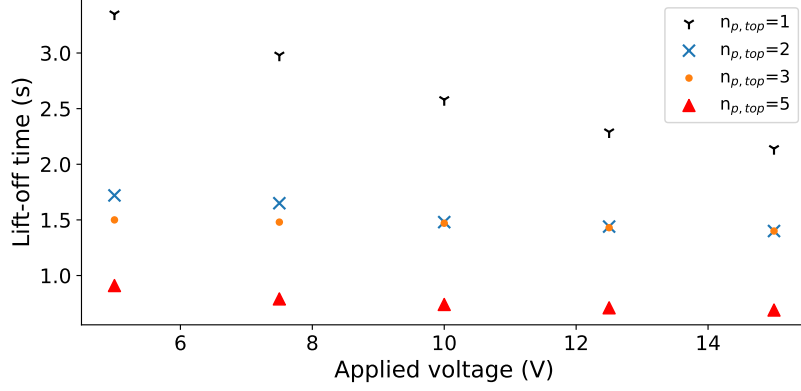


Figure 6: Lift-off times for different applied voltages. Graphs with different values of reference proton concentrations are shown in the figure, the figure shows exponential decay of the lift off time respect to the applied voltage. The effect is greater when the proton concentration at the electrode is lower.

the problem and solve it numerically. This has allowed us to perform intensive numerical testing to explore several key aspects: 1) the dependence of the bubble detachment time and volume on the Young's contact angle, 2) the detachment time, for a given Young's angle, on the applied electrical potential, 3) the dependence of the detachment time as a function of the H^+ concentration in the medium. We have concluded that the detachment time as well as the amount of gas detached depend strongly on the Young's angle. Nevertheless, if we estimate the gas production rate as the ratio between the detached volume and the detachment time, there is not a substantial dependence on Young's angle. An additional conclusion is that there is not a strong impact of the applied potential on the time of detachment. As a general rule, that time decreases with increasing voltage, but the effect is not strong. In fact, it is almost irrelevant in a medium with very low pH.

In our study we have exploited axial symmetry as a means for reducing the dimensionality of the problem and hence the computation time. The model itself can be easily applied to genuine 3D situations at a higher computational cost. There are various interesting situations to study in such setting: growth of neighbouring bubbles and study of possible screening effects, coalescence of bubble during their growth, etc. We plan to explore these issues in future publications.

References

- [1] C. Uriarte, M. A Fontelos and M. Arrayás. Phase field modeling of the detachment of bubbles from a solid substrate. *Physics of Fluids* 36, 062001 (2024).

- [2] A. Bermúdez, P. Fontán, M. Fontelos, F. Higuera and A. Rivero. Nucleation, growth and detachment of bubbles formed by reaction over surfaces. Proceedings of the 163 European Study Group with Industry (163 ESGI) 2021.
- [3] S. M. Allen and J. W. Cahn. A microscopic theory for antiphase boundary motion and its application to antiphase domain coarsening. *Acta Metallurgica*, 27(6):1085-1095, 1979.
- [4] J. W. Cahn and J. E. Hilliard, Free energy of a nonuniform system. I. Interfacial free energy, *J. Chem. Phys.* 28, 258 (1958).
- [5] Gunduz Caginalp. An analysis of a phase field model of a free boundary. *Archive for rational mechanics and analysis*, 92:205–245, 1986.
- [6] Qiang Du and Xiaobing Feng. The phase field method for geometric moving interfaces and their numerical approximations. *Handbook of Numerical Analysis*, 21:425–508, 2020.
- [7] D. Jacqmin, Calculation of Two-Phase Navier–Stokes Flows Using Phase-Field Modeling, *Journal of Computational Physics*, Volume 155, Issue 1, 10 October 1999, Pages 96-127
- [8] V.E. Badalassi, H.D. Ceniceros, S. Banerjee, Computation of multiphase systems with phase field models, *Journal of Computational Physics* 190 (2003) 371–397.
- [9] C. Eck, M. Fontelos, G. Grün, F. Klingbeil and O. Vantzos, On a phase-field model for electrowetting, *Interfaces Free Bound.* 11 (2009) 259–290.
- [10] T. Qian, X.-P. Wang and P. Sheng, A variational approach to moving contact line hydrodynamics, *J. Fluid Mech.* 564 (2006) 333–360.
- [11] M. A. Fontelos, G. Grün, U. Kindelán, F. Klingbeil, Numerical Simulation of Static and Dynamic Electrowetting, *Journal of Adhesion Science and Technology* Volume 26, (1805-1824), 2012.
- [12] Zongliang Zhang, Wei Liu and Michael L. Free, Phase-Field Modeling and Simulation of Gas Bubble Coalescence and Detachment in a Gas-Liquid Two-Phase Electrochemical System, *Journal of The Electrochemical Society*, 2020 167 013532
- [13] R. Jafari and T. Okutucu-Özyurt, Phase-Field Modeling of Vapor Bubble Growth in a Microchannel, *The Journal of Computational Multiphase Flows* Volume 7, Issue 3, 143-158 (2016)
- [14] Farhat, Mohamed ; Avellan, François, On the Detachment of a leading edge Cavitation, Proceedings of the fourth international Symposium on Cavitation, Pasadena, Ca, USA, June 2001.

- [15] W. Yin, L. Yuan ,H. Huang, Y. Cai, J. Pan, N. Sun, Q. Zhang, Q. Shu, C. Gu, Z. Zhuang, L. Wang, Strategies to accelerate bubble detachment for efficient hydrogen evolution, *Chinese Chemical Letters* 35 (2024) 108351
- [16] H. Ding, M. N. H. Gilani, P. D. M. Spelt, Sliding, pinch-off and detachment of a droplet on a wall in shear flow, *Journal of Fluid Mechanics*, Volume 644 (2010), 217-244
- [17] A. Guion , S. Afkhami , S. Zaleski, J. Buongiorno, Simulations of micro-layer formation in nucleate boiling, *International Journal of Heat and Mass Transfer*, Volume 127, Part B, December 2018, Pages 1271-1284
- [18] J. M. Gordillo and M. A. Fontelos, Satellites in the Inviscid Breakup of Bubbles, *Phys. Rev. Lett.* 98, 144503 (2007)
- [19] J. G. Eggers, M. A. Fontelos, D. Leppinen, J. H. Snoeijer, Theory of the collapsing axisymmetric cavity, *Physical Review Letters* .98, 094502 (2007).
- [20] M. Yue, H. Lambert, E. Pahon, R. Roche, S. Jemei, D. Hissel, Hydrogen energy systems: A critical review of technologies, applications, trends and challenges, *Renewable and Sustainable Energy Reviews*, Volume 146, August 2021, 111180
- [21] C. Uriarte, M. Arrayás, M. A. Fontelos, Phase field modeling of the detachment of bubbles from a solid substrate, *Physics of Fluids* 36, 062001 (2024).
- [22] COMSOL Multiphysics, v. 6.1., www.comsol.com, COMSOL AB, Stockholm, Sweden.